

# Magnetospheric accretion onto the T Tauri star AA Tauri<sup>\*</sup>

## I. Constraints from multisite spectrophotometric monitoring

J. Bouvier<sup>1</sup>, A. Chelli<sup>1</sup>, S. Allain<sup>1</sup>, L. Carrasco<sup>2,3</sup>, R. Costero<sup>3</sup>, I. Cruz-Gonzalez<sup>3</sup>, C. Dougados<sup>1</sup>, M. Fernández<sup>4</sup>, E.L. Martín<sup>5, \*\*</sup>, F. Ménard<sup>1,6</sup>, C. Mennessier<sup>1</sup>, R. Mujica<sup>2</sup>, E. Recillas<sup>2</sup>, L. Salas<sup>3</sup>, G. Schmidt<sup>7</sup>, and R. Wichmann<sup>8</sup>

<sup>1</sup> Laboratoire d'Astrophysique, Observatoire de Grenoble, Université Joseph Fourier, B.P. 53, F-38041 Grenoble Cedex 9, France (<http://www-laog.obs.ujf-grenoble.fr>)

<sup>2</sup> Instituto Nacional de Astrofísica Óptica y Electrónica, Apartado Postal 51 y 216, C.P. 72000, Puebla, Pue., México

<sup>3</sup> Instituto de Astronomía, UNAM, Ap. Postal 70264, 04510, México

<sup>4</sup> Max-Planck-Institut für Extraterrestrische Physik, Giessenbachstrasse, D-85740 Garching, Germany

<sup>5</sup> Instituto de Astrofísica de Canarias, E-38200 La Laguna, Tenerife, Spain

<sup>6</sup> Canada-France-Hawaii Telescope Corp., P.O. Box 1597, Kamuela, HI 96743, USA

<sup>7</sup> Steward Observatory The University of Arizona Tucson, AZ 85721, USA

<sup>8</sup> Landessternwarte Königstuhl, D-69117 Heidelberg, Germany

Received 2 March 1999 / Accepted 1 July 1999

**Abstract.** We have monitored the photometric, spectroscopic and polarimetric variations of the classical T Tauri star (CTTS) AA Tau over a period of a month. The light curve consists of more than 260 measurements in each of the B and V-bands over a continuous time period of 30 days and more than 180 measurements in the R and I-bands. This provides unprecedented detail of the photometric variations of a CTTS on timescales ranging from hours to weeks.

We find that AA Tau's light curve is quite unlike that of most other CTTS. It exhibits a roughly constant brightness level, interrupted by quasi-cyclic fading episodes with an amplitude of 1.4 mag in BVRI filters. We interpret this behaviour as resulting from quasi-periodic occultations of the stellar photosphere by opaque circumstellar material. The interpretation derives from the lack of significant color variations associated with the fading of the system and is strengthened by the higher polarization level measured when the system is faint.

We argue that the occultations are produced by a warp in AA Tau's inner disk which presumably results from the dynamical interaction between the disk and the stellar magnetosphere. We present a model that accounts for the observations quite naturally if we assume that the stellar magnetosphere is a large-scale dipole tilted onto the stellar rotational axis which disrupts the disk at the corotation radius. We derive the geometrical properties of AA Tau's accretion zone in the framework of this model

and constrain the location of veiling and Balmer line emitting regions.

Although AA Tau's light curve is atypical, the constraints derived here on the structure of its accretion zone may apply as well to other CTTS. It is probably only because AA Tau is seen at a peculiar inclination, close to edge-on, that occultations are conspicuous and its photometric behaviour so clearly reveals this phenomenon.

**Key words:** accretion, accretion disks – stars: circumstellar matter – stars: magnetic fields – stars: pre-main sequence – stars: pulsars: general – stars: individual: AA Tau

### 1. Introduction

T Tauri stars come in different flavours. The most intriguing of these low-mass pre-main sequence objects are surrounded by an accretion disk and simultaneously show evidence for strong winds, and are referred to as “classical” T Tauri stars (CTTS, for reviews see Bertout 1989, Calvet 1997, Hartmann 1998). Current models suggest that the accretion disk is disrupted by a strong stellar magnetic field at a distance of a few stellar radii and that accretion onto the star proceeds at free-fall velocity along magnetic field lines. Observationally, evidence for such ballistic funnel flows mainly comes from strongly redshifted absorption features in the emission line profiles of CTTS (Edwards et al. 1994, Hartmann et al. 1994, Edwards 1997) and from the detection of bright stellar spots interpreted as accretion shocks at the footpoint of the magnetic structure (Bertout et al. 1988).

While accretion takes place along magnetic field lines connecting the inner disk to the photosphere, part of the accretion flow is diverted in a wind along open magnetic field lines presumably under the effect of magnetic forces (Shu et al. 1994,

---

Send offprint requests to: J. Bouvier

<sup>\*</sup> Based on observations obtained at Haute-Provence and Pic du Midi Observatories (France), San Pedro Mártir and Cananea Observatories (México), ESO La Silla Observatory (Chile), Steward Observatory (USA) and Teide Observatory (Spain)

<sup>\*\*</sup> Present address: University of California at Berkeley, 601 Campbell Hall, CA 94720, USA

Correspondence to: [jbouvier@laog.obs.ujf-grenoble.fr](mailto:jbouvier@laog.obs.ujf-grenoble.fr)

**Table 1.** Journal of the observations

<b>Photometry</b>				
Dates	Site	Telescope	Filters	
8–15/11/95	Teide, Canarias	0.82m	BV	
9–16/11/95	San Pedro Mártir	1.52m	UBVRI	
13–20/11/95	San Pedro Mártir	2.1m	JHK	
15–28/11/95	Cananea	2.1m	BVRI	
17–30/11/95	Obs. Haute-Provence	1.2m	(U)BVRI	
22–29/11/95	San Pedro Mártir	1.52	BVRI	
20–29/11/95	ESO, La Silla	0.9m Dutch	BV	
1–10/12/95	San Pedro Mártir	1.52m	BV	
<b>Spectroscopy</b>				
Dates	Site	Telescope	Resolution	Spectral range
15–28/11/95	Cananea	2.1m	400	4000–7200
20/11–3/12–95	OHP	1.93 m	38000	3850–6800
<b>Polarimetry</b>				
Dates	Site	Telescope	Type	Spectral range
21–23/11/95	Kitt Peak	2.29m	Spectropolarimetry	4650–7150 Å
23–29/11/95	Pic-du-Midi	2m	Aperture	V

Paatz & Camenzind 1996, Ferreira 1997). Königl (1991) suggested that accretion onto magnetic T Tauri stars (TTS) could also account for their low rotation rates, typically an order of magnitude lower than break-up velocity (Hartmann & Stauffer 1989). Schematically, magnetic field lines connecting the star to the disk beyond the corotation radius exert a negative torque onto the star while accretion tends to spin it up. When the disk truncation radius lies in the vicinity of the corotation radius, the net torque on the star vanishes and the star evolves at roughly constant angular velocity (Collier Cameron & Campbell 1993, Armitage & Clarke 1996). Observational evidence for the regulation of TTS rotation rates by this mechanism has been reported by Bouvier et al. (1993), Edwards et al. (1993) and Choi & Herbst (1996), though alternative interpretations have been suggested by Popham (1996) and the recent study by Stassun et al. (1999) of the rotational periods of TTS in Orion has brought some dissenting opinions.

One of the key assumptions of magnetospheric accretion models is the topology and the strength of the stellar magnetic field. It is often assumed that the stellar magnetosphere is a large-scale dipole aligned with the stellar rotational axis (but see King & Regev 1994 for an alternative) and recent Zeeman measurements indicate kilogauss magnetic fields at the surface of T Tauri stars, strong enough to disrupt the inner disk at a few stellar radii (Guenther et al. 1999, Johns-Krull et al. 1999). Yet, the actual geometry and temporal evolution of TTS magnetospheres still remain poorly constrained.

With the hope to clarify the geometry of the accretion zone in T Tauri stars, we have performed a multisite campaign on a sample of CTTS aimed at simultaneously monitoring their photometric, spectroscopic and polarimetric variations over several rotational periods. We report here the results obtained on the CTTS AA Tau. Sect. 2 briefly describes the organization of the multisite campaign. Sect. 3 presents the photometric, spec-

troscopic and polarimetric variations recorded for AA Tau on timescales ranging from a few hours to several weeks. In Sect. 4, we discuss various interpretations of AA Tau's variability and conclude that it most likely results from recurrent occultations of the stellar photosphere by orbiting circumstellar material. Finally, a tentative model for AA Tau's accretion zone is presented in Sect. 5 and implications for the magnetospheric accretion process are discussed.

## 2. Observations

The Journal of Observations is given in Table 1. The dates listed are those of the observing runs, some of which were heavily hampered by bad weather. This is the case in particular for the spectroscopic observations at OHP during which only 2 high-resolution spectra were obtained. Due to the large number of sites involved in this campaign, we give here only a brief generic account of data acquisition and reduction procedures.

All photometric observations were obtained with CCD devices using UBVRI filters or a subset thereof. Data acquisition and reduction techniques are the same as those used for previous COYOTES campaigns (see Bouvier et al. 1995). Images were bias subtracted and flat-field corrected in a standard manner. Using IRAF/DAOPHOT, PSF photometry was performed on AA Tau as well as on 3 comparison stars located less than 2 arcmin away from AA Tau (no. 1125-01689518, 1125-01691043 and 1125-01691176 in the USNO2 catalogue) and which were used to compute differential light curves. The absolute photometric calibration in the Cousins system was done by observing Landolt's (1983) standard stars at ESO, OHP and San Pedro Mártir. Photometric errors are of order of 0.02 magnitudes or less in all filters for differential photometry at each site but increase to about 0.05 mag rms when photometry from all sites is combined, probably due to slight differences in the filter sets. These

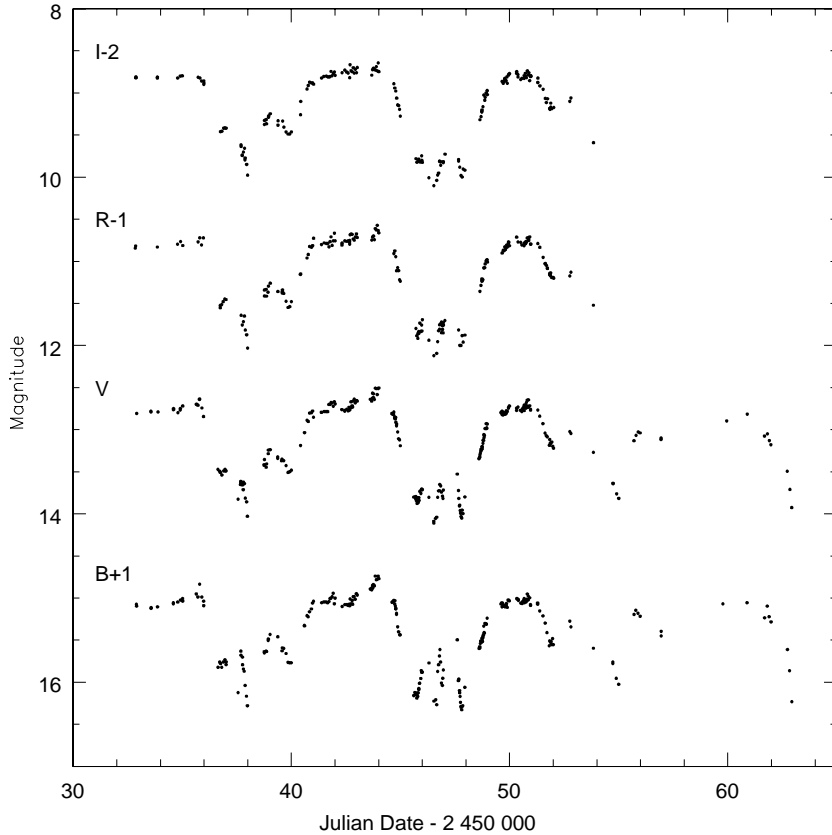


**Fig. 1.** Photometric variations of AA Tau in the BVRI filters. The BRI light curves have been shifted for clarity.

rms errors computed as the standard deviation of the comparison stars referenced against each other as a control are probably conservative since these stars are about 2 magnitudes fainter than AA Tau.

JHK photometry was obtained with the infrared camera CAMILA (Cruz-González et al., 1994) at the 2.1m telescope of the Observatorio Astronómico Nacional at San Pedro Mártir, B.C. (México). The UKIRT standards FS8 and FS9 were observed for photometric calibration leading to a mean internal photometric error in each band between 0.02 to 0.05 mag, the latter being probably closer to the absolute photometric precision.

Low-resolution spectroscopy ( $R \approx 400$ ) was obtained at the 2.1m telescope of the Guillermo Haro Observatory (INOAE), Cananea (México), equipped with the LFOSC spectrograph (Zickgraf et al. 1997). From Nov. 15 to 28, 1995, 97 spectra of AA Tau were obtained, with a S/N ratio ranging from about 50 to 100. In addition, 2 high-resolution spectra ( $R=38000$ ) were obtained at the Haute-Provence Observatory using the ELODIE spectrograph (Baranne et al. 1996).

V-band aperture polarimetry was performed from Nov. 23 to 29, 1995 at the 2m TBL telescope of Pic-du-Midi Observatory using the Sterenn polarimeter. In addition, linear spectropolarimetry covering the wavelength range  $\lambda\lambda 4650\text{--}7150$  at a resolution of  $8 \text{ \AA}$  was obtained at the Kitt Peak National Observatory on Nov. 21–23, 1995, with the CCD spectropolarimeter described by Schmidt et al. (1992). Standard calibration procedures included observations of stellar flux standards obtained

with the same instrumental setup and of polarization standard stars during the run. Instrumental polarization was measured to be negligible and is not corrected for.

### 3. Results

We report in this section the main features of AA Tau’s photometric, spectroscopic and polarimetric variability.

#### 3.1. Photometric variability

The light curve<sup>1</sup> of AA Tau in the BVRI filters is shown in Fig. 1. The U-band light curve contains only 32 measurements and is not shown.

The most striking feature of AA Tau’s light curve is the repeated occurrence of deep and wide brightness minima. The best sampled ones occur around around day 38 and 47 (all dates correspond to J.D. - 2 450 000). On each side of these minima, the star lies at a roughly constant brightness level. Remarkably, the depth of the minima is about the same at all wavelengths from B to I, with  $\Delta m \approx 1.4$  mag to within 0.1 mag. Hence, the large brightness variations occur without significant color changes of the system. This behaviour is also illustrated in Fig. 2, where the V and B-V light curves are shown: as the system goes through bright and faint states, the B-V color changes by less than 0.1 mag on a timescale of weeks. Furthermore, the system tends

<sup>1</sup> Tables of photometric measurements are available electronically at CDS Strasbourg.

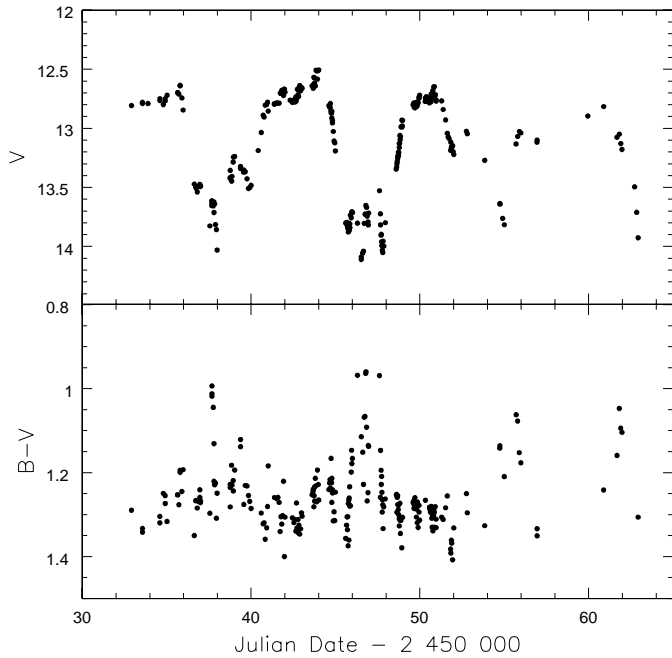


**Fig. 2.** The V and (B-V) photometric variations of AA Tau. The B-V light curve has been computed by pairing B and V measurements obtained no more than 15 minutes apart.

to be bluer when fainter. Superimposed on this midterm behaviour, rapid color changes occur within the luminosity dips with the system suddenly turning much bluer on a timescale of a few hours (e.g., on day 37.5 and 46–48). These blue excursions appear to be correlated with transient brightening events primarily observed in the faint state, while in the bright state the short-term photometric variability seems much smoother.

The fading episodes appear to repeat themselves on a characteristic timescale of about a week. A CLEAN-periodogram analysis (Roberts et al. 1987) indicates a period of  $P_{phot} = 8.3 \pm 0.05$  days in the BVRI filters, while the string-length method (Dworetzky 1983) yields  $P_{phot} = 8.6 \pm 0.1$  days. These estimates are consistent with the previously reported photometric period of 8.2 days (Vrba et al. 1989, Shevchenko et al. 1991). Light curves folded in phase with a period of 8.5 days are shown in Fig. 3. Even though the variations are obviously not perfectly reproducible from one cycle to the next, the existence of a period—or characteristic timescale if not a strict period—is strongly supported by the overall coherency of the phase diagrams.

Near-IR measurements (Table 2) were obtained on AA Tau in the JHK filters over 6 nights encompassing part of the first fading episode and the return of the system to the bright state. The near-IR photometric variations are correlated with the visual ones albeit with a much lower photometric amplitude, decreasing from about 0.7 mag at J to 0.45 mag at K. Spectral energy distributions (SED) constructed by combining the visual and near-IR photometry are shown in Fig. 4 for AA Tau in the bright and faint states. A K7 photosphere reddened by 0.8 mag (see Appendix) has been fitted to the SEDs and reveals the presence of blue and near-IR excesses at all phases of the photometric cycle. While the photospheric flux decreases by a factor of about

**Table 2.** JHK photometry

Date	J	J-H	H-K
37.309	9.70	0.84	0.50
37.376	9.65	0.82	0.48
38.308	9.94	—	—
38.378	9.99	0.85	0.59
39.328	9.69	0.85	0.51
39.395	9.68	0.87	0.46
40.340	9.81	0.85	0.55
40.523	9.88	0.92	0.44
41.353	9.38	0.81	0.43
43.381	9.30	0.70	0.49

3.5 between the bright and faint states, we find that the near-IR excess flux remains constant along the photometric cycle. This is consistent with the near-IR study of Skrutskie et al. (1996) who found that AA Tau’s behaviour in an E(H-K)–E(J-H) diagram was indicative of a relative brightness change between the photosphere and the inner disk. In contrast, the excess flux in the B band does decrease by a factor of about 3 as the system fades (see Fig. 4). The physical mechanism responsible for the variations of the photospheric flux must then simultaneously and nearly equally affect the blue excess emitting region.

### 3.2. Spectroscopic variability

Low-resolution spectra were continuously obtained for AA Tau over more than 2 weeks covering several brightness minima and maxima. In a given luminosity state, the individual spectra are similar. We therefore averaged a set of spectra taken during AA Tau’s fading episodes and another set obtained at maximum brightness. The resulting average spectra in the bright and faint states are shown in Fig. 5.

We do not detect any significant change in AA Tau’s spectral type within a couple of subclasses during the photometric cycle. There are however a number of differences between the 2 spectra. The most obvious is the increase of Balmer lines equivalent width at minimum brightness. The temporal variations of  $EW(H_\alpha)$  and  $EW(H_\beta)$  are shown in Fig. 6. They appear to be inversely correlated with the system’s brightness, being enhanced during the fading episodes. Fig. 6 also shows the variations of the  $H_\alpha$  and  $H_\beta$  line fluxes<sup>2</sup>. From day 38 to about 48, the  $H_\alpha$  line flux seems to correlate with the continuum flux though this correlation tends to disappear thereafter. This indicates that the enhanced equivalent widths observed in the faint state at least partly result from a contrast effect as the photospheric flux weakens. The  $H_\beta$  line has a more erratic behaviour, exhibiting the largest flux at both minimum and maximum brightness.

<sup>2</sup> The line fluxes were computed by combining photometric and spectroscopic measurements taken less than half an hour apart as:  $F(H_\alpha) \propto EW(H_\alpha) \cdot 10^{-0.4m_R}$  and  $F(H_\beta) \propto EW(H_\beta) \cdot 10^{-0.4m_B}$ , where  $m_R$  and  $m_B$  are the magnitudes of the system in the R and B-bands, respectively.

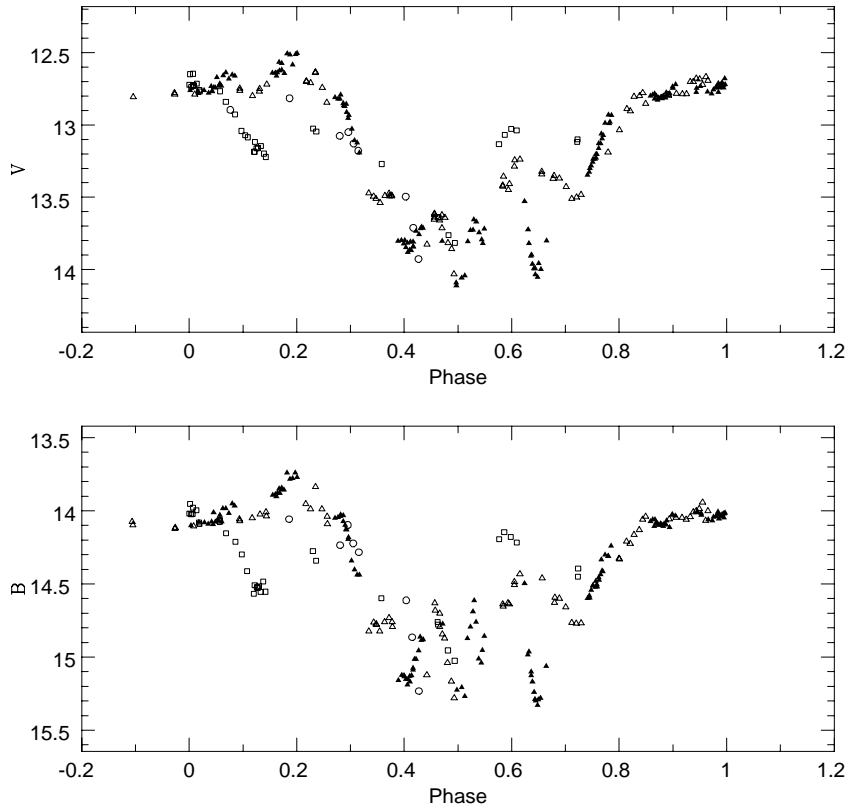


**Fig. 3.** Phase diagrams for AA Tau’s V (upper) and B (lower) light curves for a period of 8.5 days. The 4 photometric cycles sampled by the light curve are shown by different symbols: J.D. 33.8–42.3 (empty triangles), J.D. 42.3–50.8 (filled triangles), J.D. 50.8–59.3 (empty squares), J.D. 59.3–67.8 (empty dots).

**Table 3.** V-band polarization measurements

Date	$\phi_{obs}$	P (%)	$\theta$ ( $^{\circ}$ )
42.823	0.03	0.72 (0.03)	25.0 (0.8)
43.979	0.17	0.70 (0.03)	24.5 (0.8)
44.891	0.28	1.06 (0.03)	14.8 (0.8)
48.547	0.71	1.33 (0.13)	2.2 (2.4)
49.525	0.82	0.60 (0.09)	20.3 (3.7)
49.676	0.84	0.80 (0.21)	20.8 (6.5)
50.638	0.95	0.84 (0.10)	27.5 (2.9)

AA Tau’s spectrum also exhibits a shallower continuum slope as well as shallower photospheric features in the faint state. This suggests that the photospheric spectrum is more heavily veiled by a source of blue continuum emission at minimum brightness. From the 2 high-resolution spectra obtained around day 50.6, at a time when the system was at maximum brightness, we measure a weak veiling amounting to  $r_{0.6\mu} = 0.15 \pm 0.05$ . Published data provides further evidence that the veiling does increase when the system dims. Hartigan et al. (1990, 1995) repeatedly found that the veiling measured at  $0.6 \mu\text{m}$  and the equivalent width of the [OI] $\lambda 6300$  line increase simultaneously in AA Tau’s spectrum on a timescale of days. Since [OI] lines are thought to form far away from the star, their intrinsic flux is not expected to vary on such a short timescale. Therefore, an enhanced EW[OI] merely reflects a dimmer continuum, at a time when the veiling is observed to be larger.

For the sake of completeness, Fig. 7 shows the  $H_{\alpha}$  and  $H_{\beta}$  line profiles extracted from the 2 high-resolution spectra recorded

during the campaign. The profiles exhibit a deep central absorption and are qualitatively similar to those previously reported in the literature (Edwards et al. 1994). From a cross-correlation analysis of the photospheric spectrum, we derive  $v \sin i = 11 \pm 1.5 \text{ km s}^{-1}$  and  $V_r = 16.5 \pm 0.3 \text{ km s}^{-1}$  for AA Tau’s projected rotational velocity and heliocentric radial velocity, respectively.

### 3.3. Polarimetric variability

Polarimetric measurements in the V-band continuum are listed in Table 3. They cover AA Tau’s maximum brightness level as well as the very start and the very end of the second fading episode but unfortunately missed AA Tau’s faintest luminosity level.

The polarization level in the continuum increases from about 0.7% to 1.3% as the system dims. This suggests that direct (unpolarized) photospheric light is depressed around minimum brightness relative to the polarized stellar photons scattered back to the observer by circumstellar dust. This result together with AA Tau’s behaviour in the near-IR is consistent with its photometric variability being primarily driven by variations of the photospheric flux.

The position angle varies as well along the photometric cycle, probably reflecting the changing illumination of the scattering region as the system rotates (Stassun & Wood 1999). Note that the polarization level and angle measured after the fading episode are similar to those measured before, which suggests possibly periodic polarimetric variations on a timescale similar

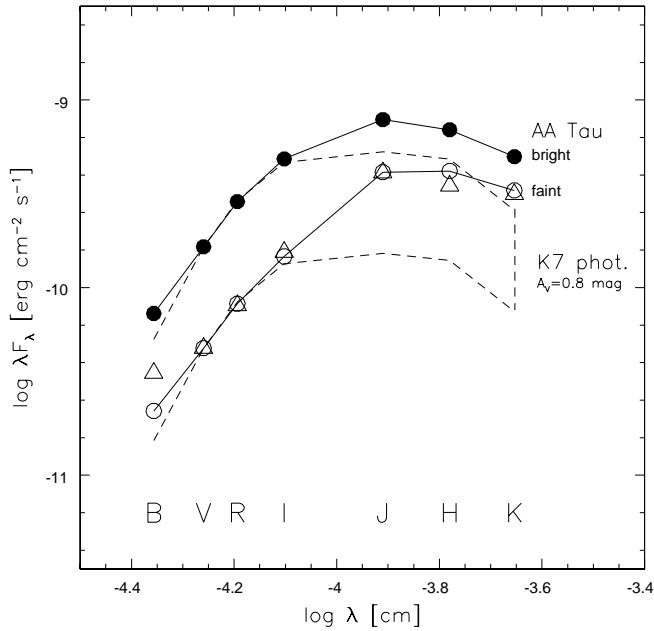


**Fig. 4.** The observed spectral energy distribution (SED) of AA Tau in the bright and faint states (filled and empty dots, respectively). The dashed lines show the SED of two K7 photospheres, both reddened by  $A_V = 0.8$  mag and normalized to the V flux. The visual extinction, as measured by  $E(V-R)$ , does not appear to change as the system dims. The triangles show the fluxes computed from the K7 photosphere in the faint state and adding the blue and near-IR excess fluxes measured in the bright state. The near-IR part of this synthetic SED matches that of AA Tau in the faint state which indicates that the near-IR flux is not significantly depressed as the system dims. In contrast, the blue excess flux is weaker in the faint state than in the bright one.

to the photometric period. However, the data are too sparse to firmly establish such a behaviour.

#### 4. Interpretation

AA Tau appears to be a rather typical CTTS: K7 spectral type, mild IR excess, weak veiling, moderate strength of the emission-line spectrum, average visual extinction. It is not known to be a binary either from spectroscopic monitoring or from high-resolution imaging. Yet, the overall photometric behaviour of AA Tau described in the previous section is quite atypical of T Tauri stars, classical and weak-line alike, and somewhat reminiscent of the photometric variations of the UXor subclass of Herbig Ae-Be stars (though UXors do not exhibit week timescale periodicities in their photometric variations, see Herbst et al. 1994). What makes AA Tau so peculiar is primarily the near lack of color variations while the system's flux changes by more than 1 magnitude. Furthermore, the small color change that occurs indicates that the system tends to be bluer when fainter. In contrast, almost all T Tauri stars become redder when fainter, with their color variations being primarily driven by cold or hot spots (Herbst et al. 1994). The only other clear cases of T Tauri stars exhibiting either nearly achromatic photometric variations or a blue turnaround in colors at minimum brightness are RY

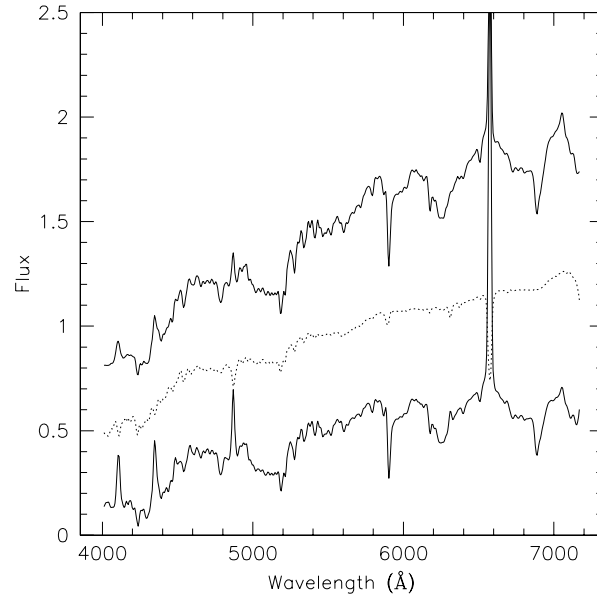


**Fig. 5.** Average low-resolution spectra of AA Tau at maximum (top) and minimum (bottom) brightness. The upper spectrum is an average of 42 spectra recorded in the bright state from day 40.5 to 44.0 and from day 49.5 to 51.0. The lower one is an average of 20 spectra obtained during the luminosity dip between day 45.0 and 48.0. Both spectra were normalized to unity at  $0.55 \mu\text{m}$  and shifted by  $\pm 0.5$  for clarity. The dotted curve is the ratio between the bright and faint states spectra.

Tau prior to its 1983 outburst (Eaton & Herbst 1995) and RY Lupi (Gahm et al. 1989).

In this section, we will discuss in turn different possible causes for the observed photometric, spectroscopic and polarimetric variations of AA Tau, namely: eclipses in a short-period binary system, rotational modulation by spots, and variable circumstellar extinction. The stellar parameters used throughout this section are discussed in the Appendix. We summarize below the results that have to be explained:

- 1a. The photometric variations are nearly achromatic with an amplitude of about 1.4 mag at visible wavelengths and quasi-periodic on a timescale of 8.5 days.
- 1b. Transient brightening episodes are observed on a timescale of a few hours associated with a sudden blueing of the system's colors. These episodes are primarily observed during the faint state of the system.
- 1c. The near-IR excess flux appears to remain constant along the photometric cycle while the photospheric flux varies by more than a factor of 3 at both visible and near-IR wavelengths.
- 1d. The blue excess flux decreases by a nearly similar amount as the photospheric flux when the system fades. At minimum brightness, the system appears only 0.1 mag bluer on average than in the bright state.
- 2a. AA Tau's spectral type does not significantly change during the photometric cycle.
- 2b. Photospheric features appear to become shallower during the fading episodes, which suggests that the veiling is stronger when the system is faint.

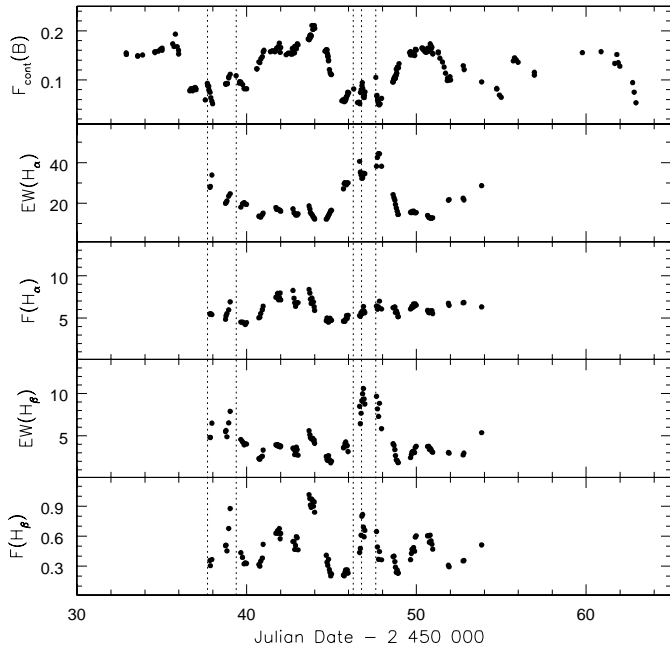


**Fig. 6.** Temporal variations of the  $H_\alpha$  and  $H_\beta$  lines equivalent width ( $\text{\AA}$ ) and flux ( $10^{-13} \text{ erg s}^{-1} \text{ cm}^{-2}$ ). The measurement uncertainty is  $0.5 \text{ \AA}$  for  $\text{EW}(H_\alpha)$  and  $0.8 \text{ \AA}$  or less for  $\text{EW}(H_\beta)$ . The upper panel shows the variations of the continuum flux in the B filter ( $10^{-13} \text{ erg s}^{-1} \text{ cm}^{-2} \text{ \AA}^{-1}$ ). The dotted lines indicate the occurrence of transient blueing episodes at minimum brightness (see Fig. 2)

2c. Balmer line equivalent widths, from  $H_\alpha$  to  $H_\delta$ , are inversely correlated with the system's brightness, being larger when the system is fainter (Fig. 5). However, the  $H_\alpha$  line flux at least partly correlates with the continuum flux.

3a. The level of polarization in the continuum increases as the system fades. The position angle appears to rotate along the photometric cycle.

#### 4.1. An eclipsing binary

The quasi-periodic and achromatic fading episodes of AA Tau in the optical range and the flat brightness maxima could conceivably result from partial eclipses in a short-period binary system. Assuming an 8.5d orbital period and a  $0.8M_\odot$  primary, we have:

$$K_1 = 10^{7/3} P_{orb}^{-1/3} M_1^{1/3} q(1+q)^{-2/3} \simeq 10^2 \cdot q \cdot (1+q)^{-2/3}$$

where  $K_1$  is the semi-amplitude of the radial velocity variations expected for the primary in  $\text{kms}^{-1}$ ,  $P_{orb}$  is the orbital period in days,  $M_1$  is the mass of the primary in solar masses,  $q = M_2/M_1$  is the mass ratio between the secondary and the primary, and we assumed a circular orbit with  $\sin i = 1$ . For mass ratios between 0.1 and 1, the peak-to-peak range of radial velocity variations would then lie between 18 and  $134 \text{ kms}^{-1}$  for the primary.

Hartmann et al. (1986) derived  $V_r = 16.1 \pm 2.1 \text{ kms}^{-1}$  from 4 high-resolution spectra, a value close to the mean radial velocities of T Tauri stars in Taurus, and did not report any significant velocity variations beyond error bars. From our 2 high resolution

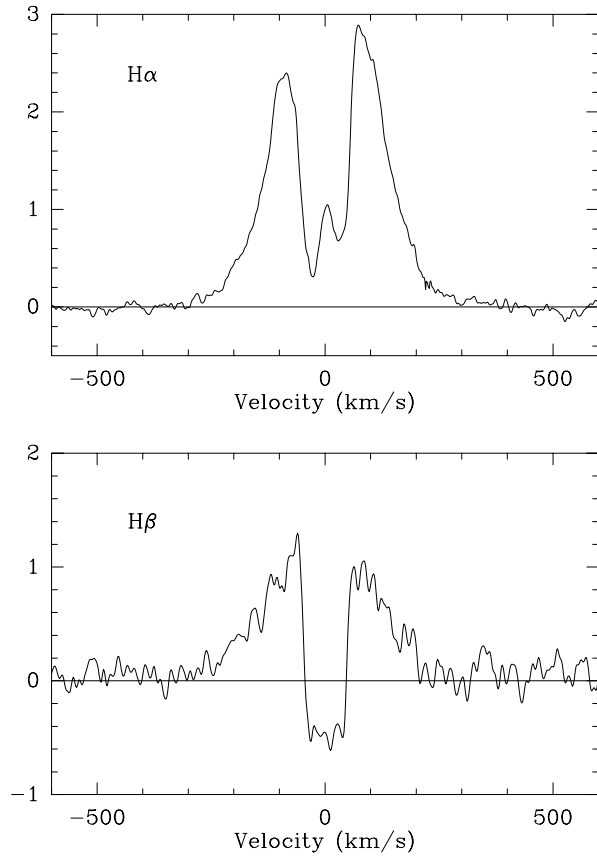


**Fig. 7.** The  $H_\alpha$  and  $H_\beta$  line profiles of AA Tau observed on day 50.6. Residual emission line profiles were computed by normalizing the nearby continuum to one and subtracting the normalized spectrum of a K7 template (HD 201092). A veiling of 0.15, as measured in AA Tau's photospheric spectrum, was added to the K7 template before subtraction.

spectra, we measured  $V_r = 16.5 \pm 0.3 \text{ kms}^{-1}$ . Furthermore, R. Mathieu (private communication) obtained 19 high-resolution spectroscopic observations of AA Tau over 2100 days. The peak-to-peak range of their observations is  $9 \text{ kms}^{-1}$  with a dispersion of  $2 \text{ kms}^{-1}$ . If interpreted as orbital motion, these results would restrict the binary mass ratio to 0.05 or lower, implying a mass of about 40 Jupiter masses or less for the companion.

From radial velocity measurements alone, we thus cannot totally exclude that AA Tau is an eclipsing binary system with either a low-mass brown dwarf or a giant planet companion orbiting at a distance of about  $9R_*$ . According to Baraffe et al.'s (1998) models, a  $0.04M_\odot$  brown dwarf at an age of 2 Myr would have an effective temperature of 2800 K, a luminosity of about  $0.01L_\odot$  and a radius of about  $0.5R_\odot$ . Such a low-mass companion would hardly contribute to the flux of the system in the optical, thus accounting for the achromatism of the eclipses at visible wavelengths, and could possibly start to contribute at near-IR wavelengths, consistent with shallower eclipses in the JHK bands.

However, this interpretation faces obvious difficulties. Given the radius and the orbiting distance of the putative com-

panion, it is difficult to account for both the duration and the depth of the observed luminosity dips, as well as for the apparent phase changes occurring from one photometric cycle to the next. High-resolution spectroscopic monitoring of AA Tau over several photometric cycles is needed to investigate possible periodic variations of its radial velocity. Pending these observations, we consider this interpretation as highly unlikely and do not discuss it further in this paper.

#### 4.2. Stellar spots

Rotational modulation by stellar spots has provided a successful interpretative framework for the photometric variability of many TTS, especially in cases of periodic or quasi-periodic light variations (cf. Herbst et al. 1994 and references therein). In AA Tau's case, a single hot spot can be readily dismissed as the origin of the modulation as it would induce strong color variations which are not observed. We therefore first explore whether a single giant cool spot could produce the light curve. In order to maximize the photometric amplitude, we assume that the star is seen edge-on and that the spot's center is located at the stellar equator. Then, the spot faces the observer at maximum visibility and disappears on the hidden stellar hemisphere at the opposite phase. In order to minimize color variations, we formally assign a zero temperature to the spot. Small color changes will still result due to limb-darkening effects (Dorren 1987) and we adopt BVRI limb-darkening coefficients from Claret's models (1998) for  $T_{eff} = 4000$  K and  $\log g = 4$ .

The resulting synthetic light-curve computed from the spot model described in Bouvier et al. (1993) is illustrated in Fig. 8. In order to reproduce the photometric amplitudes, the projected spot area has to cover at least 70% of the stellar hemisphere. Though small, modulation of the V-I color is still significant. Color variations can be further reduced by assuming that a small hot spot coexists with the giant cool spot at the stellar surface. For the sake of illustration, we computed a model with the same giant cool spot as before and adding an 8000 K spot covering 0.1% of the same stellar hemisphere. The results are shown in Fig. 8. No color variations remain in (V-R) and (V-I), and the system effectively turns bluer in (B-V) when fainter due to the larger contribution of the hot spot at short wavelengths.

The spot models derived above provide a reasonable fit to the overall shape of the light-curve and are consistent with the lack of color variations. However, since almost any quasi-periodic light curve can be reproduced by spot modulation, the main issue is not whether a spot model succeeds in accounting for AA Tau's light curve but whether the model appears physically plausible. In AA Tau's case, one has to assume the existence a huge single cool spot located at a low latitude ( $\leq 30^\circ$ ) on one stellar hemisphere, the other hemisphere being immaculate. Moreover, if the variations in photospheric flux are to remain achromatic at near-IR wavelengths, as suggested by Fig. 4, the spot has to be at least 2500 K colder than the  $T_{eff} = 4030$  K photosphere. Assuming a magnetic origin for the spot, this would imply quite a peculiar topology for the surface magnetic field. Such a huge dark spot could be associated with the magnetic pole of a large-

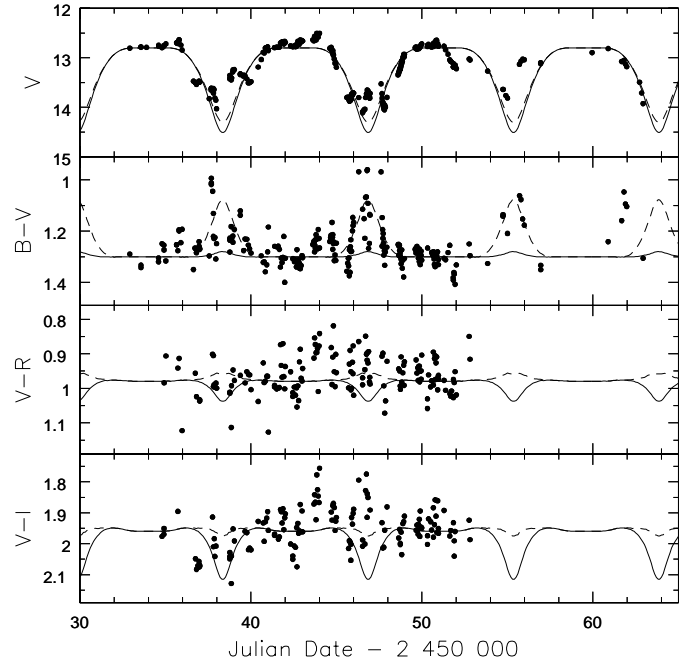


**Fig. 8.** Spot models for AA Tau light-curves. The solid-line illustrates the model for a single dark spot covering 70% of a stellar hemisphere while the dashed line additionally assumes the existence of a tiny 8000 K spot located on the same hemisphere (see text).

scale dipolar field, but a symmetric spot would then be expected on the opposite hemisphere. The photometric period of 8.5 days cannot result from symmetric spots since it would then imply a rotational period of 17 days, which conflicts with AA Tau's  $v \sin i$ . Alternatively, the dark spot may consist of many smaller active regions, but it is then difficult to imagine a reason why all these active regions would concentrate onto a single stellar hemisphere.

The spot interpretation could be further tested by Doppler imaging techniques and high-resolution spectroscopic monitoring of the system is planned for the fall 1999. Meanwhile, on the basis of the difficulties outlined above, we consider the spot interpretation as physically unlikely.

#### 4.3. Variable circumstellar extinction

Variable circumstellar extinction might offer a more straightforward explanation to AA Tau's photometric variability. The recurrent fading episodes would then be interpreted as resulting from an orbiting clump of circumstellar material which periodically intercepts the line of sight to the star. Neutral extinction is required to account for the achromatic variations. This could result either from dusty material with grain sizes significantly larger than  $1 \mu\text{m}$  or from completely opaque material leading to partial occultations of the stellar photosphere. We will argue below that the occulting material is most likely connected to the disk and that the column density at the location of the dust clump is most probably large enough to make it completely optically thick.

Assuming that the circumstellar material orbits the star in keplerian motion, the 8.5d photometric period would locate it at a radial distance of

$$r_c = (P_{kep}/2\pi)^{2/3}(GM_\star)^{1/3} = 8.8R_\star$$

with  $M_\star = 0.8M_\odot$  and  $R_\star = 1.85R_\odot$ . At this distance from the central star the temperature of irradiated dust grains is in the order of:

$$T_d \simeq \left(\frac{L_\star}{16\pi\sigma r_c^2}\right)^{1/4} \simeq 1000 K$$

with  $L_\star = 0.8L_\odot$ . Furthermore, for a typical mass-accretion rate of  $10^{-8}M_\odot\text{yr}^{-1}$ , viscous heating in the disk also leads to a temperature of about 1000 K at  $8.8R_\star$  (Papaloizou & Terquem 1999). Hence dust grains are expected to survive at this radius.

The duration of the luminosity dips in AA Tau’s light curve amount to more than half the photometric period (5.1d and 8.5d, respectively). If due to circumstellar extinction, it implies that the obscuring material is quite elongated azimuthally, extending over *at least*  $\pi$  radians around the central star. At the same time, only about 2/3 of the photosphere must be occulted at minimum light in order to account for the photometric amplitudes. Altogether, this suggests that the obscuring material has an arc-like shape of limited vertical extent and large azimuthal extension.

We tentatively identify this structure as an inner disk warp, i.e., a non-axisymmetric thickening of AA Tau’s inner disk in the vertical direction. At a distance of  $8.8R_\star$ , the “inflated” disk is likely to intercept the line of sight to the star and thus produce occultations only if the system is seen at a high inclination. Various clues support this view:

- AA Tau’s [OI] $\lambda$ 6300 line profile exhibits a single, slightly blueshifted ( $-7\text{kms}^{-1}$ ) and nearly symmetric component (Hirth et al. 1997, Hartigan et al. 1995). In most CTTS, the [OI] line profile is double-peaked, consisting of a low-velocity component and an additional, strongly blueshifted component, up to a velocity of  $-250\text{kms}^{-1}$  in extreme cases. The latter is thought to occur in a high velocity jet propagating in a direction perpendicular to the disk plane. Another diagnostic of high velocity jets is the [NII] $\lambda$ 6530 line and Hirth et al. (1997) reported that all CTTS exhibiting [NII] $\lambda$ 6530 line emission systematically display a highly blueshifted [OI] component. AA Tau is an exception since [NII] emission is clearly seen in its spectrum but the [OI] emission peak is hardly blueshifted. This suggests that AA Tau’s jet lies in the plane of the sky, i.e., that the system is seen close to edge-on.
- AA Tau’s Balmer emission line profiles exhibit a deep central absorption. If these lines are formed in free-falling accretion columns (Hartmann et al. 1994, Muzerolle et al. 1998), the central absorption must originate from the top of the accretion column before the flow gets significantly accelerated. Kwan (1997) suggested that deep central absorptions in Balmer lines arise from gas located at a few stellar radii, close to the disk midplane. In order to intercept this region, the line of sight to AA Tau must be grazing the upper layers of the disk.

- AA Tau’s  $v \sin i$  amounts to  $11\text{kms}^{-1}$ . With  $R_\star = 1.85R_\odot$  and assuming  $\sin i = 1$ , this leads to a rotational period of 8.2 days, consistent with previously reported periods in AA Tau’s light curve (Vrba et al. 1989; Shevchenko et al. 1991).
- Basri & Bertout (1989) derived an inclination of  $70^\circ$  for AA Tau’s disk axis from the modeling of its spectral energy distribution from UV to mid-IR wavelengths.

These independent clues all suggest that AA Tau is seen close to edge-on. The dusty material assumed to be responsible for the occultations must then orbit in a plane close to the equatorial plane of the system which in turn strongly suggests that it is physically connected to the disk.

The geometry of the occulting material is further constrained by the flat luminosity maxima observed in AA Tau’s light curve which indicate that the star is fully visible between successive occultations. We computed a synthetic light curve assuming that the inner disk height varies with azimuth as:  $h(\phi) = h_{max} \left| \cos \left( \frac{\phi - \phi_0}{2} \right) \right|$ , where  $\phi_0$  is the azimuth of the disk’s maximum thickness and corresponds to the photometric phase of the center of the occultation. With this prescription, the height of the inner disk smoothly decreases from  $h_{max}$  at  $\phi_0$  to zero at the opposite azimuth. The synthetic light curve is shown in Fig. 9. It merely illustrates the varying degree of occultation experienced by the central star as the system rotates. The occulting material is an optically thick disk “wall” located at a distance  $r_c = 8.8R_\star$ , extending from the disk midplane upwards to  $h_{max} = 0.3r_c$  and whose height varies with azimuth as described above. It is seen that the main features of AA Tau’s photometric variations, namely the quasi-cyclicity, depth, overall shape and duration of the luminosity dips are roughly recovered by this occultation model.

Finally, we derive a rough estimate of the optical depth of the absorbing material on the line of sight in the framework of this model:  $\tau_\lambda = \kappa_\lambda \rho \Delta r$ , where  $\kappa_\lambda$  is the opacity of interstellar-like material,  $\rho$  is the local gas density, and  $\Delta r$  is the radial extent of the dusty material on the line of sight. Assuming that the circumstellar material is in keplerian orbit around the star, an upper limit to  $\Delta r$  is derived from the phase changes occurring in the light curve between successive occultations. From Fig. 3, we conservatively estimate that the photometric phase is conserved to better than 20%. We then have:

$$\frac{\Delta P_{kep}}{P_{kep}} = \frac{3}{2} \frac{\Delta r}{r} \leq 0.2$$

which leads to  $\Delta r \leq 0.1r_c \simeq 10^{11}$  cm. The absorbing structure thus appears as a sharply defined slab of dusty material in the radial direction resembling an inner disk “wall”.

A crude estimate of the local gas density  $\rho$  is obtained as follows. From the occultation model above we derived  $h_{max}/r_c \simeq 0.3$ . The local gas density is estimated as  $\rho \simeq \Sigma_d(r_c)/2h_{max}$  where  $\Sigma_d(r_c)$  is the surface density of AA Tau’s disk at the radius  $r_c \simeq 0.1$  AU. For a mass-accretion rate between a few  $10^{-9}$  and  $10^{-8}M_\odot\text{yr}^{-1}$  as derived for AA Tau (Basri & Bertout 1989, Gullbring et al. 1998),

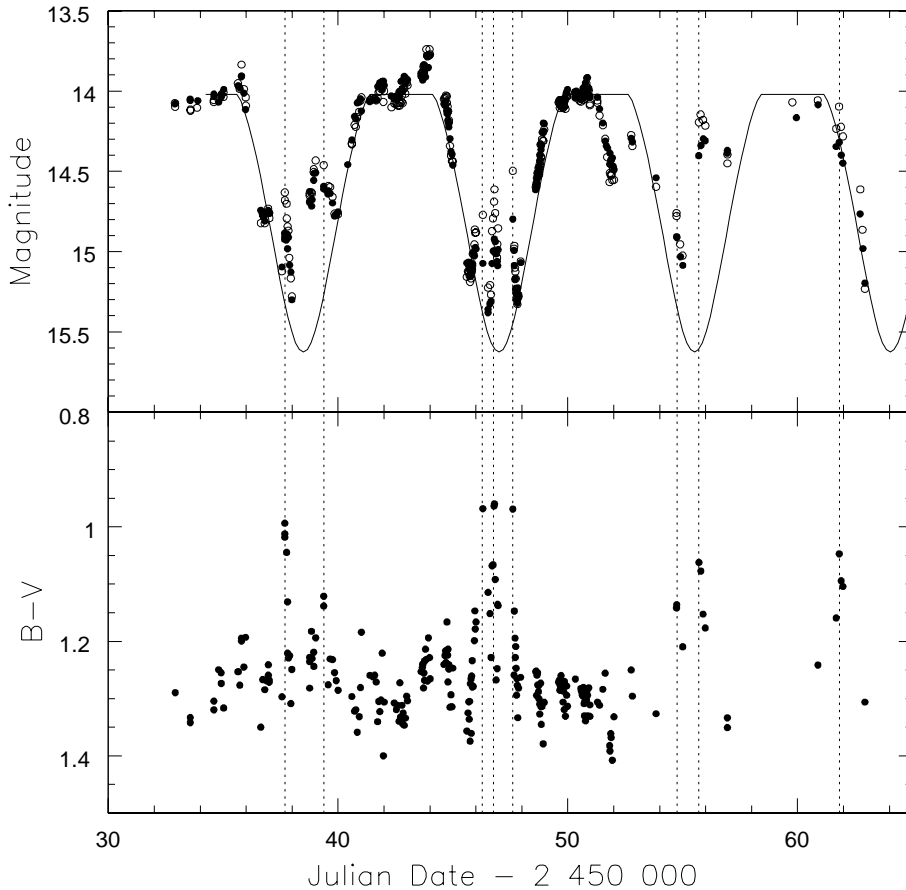


**Fig. 9.** Upper panel: AA Tau’s observed V-band (filled dots) and B-band (empty dots) light curve compared to the light curve derived from the occultation model (solid curve). The V-band light curve has been shifted by +1.27 mag to superimpose it onto the B-band one. The model light-curve is computed for  $M_* = 0.8M_\odot$ ,  $R_* = 1.8R_\odot$ ,  $r_c = 8.8R_*$ ,  $h_{max} = 2.7R_*$  (see text) and the system is seen at an inclination of  $75^\circ$  (see Appendix). Lower panel: AA Tau’s B-V light curve. Note how the system turns suddenly bluer during the occultations as transient brightening episodes are observed.

$\Sigma_d(0.1 \text{ AU})$  ranges between 100 and  $10^4 \text{ g cm}^{-2}$  depending on the assumed disk’s viscosity (Papaloizou & Terquem 1999). We conservatively adopt  $\Sigma_d(0.1\text{AU}) = 100 \text{ g cm}^{-2}$  which leads to a gas column density on the line of sight of  $N_H = \rho\Delta r \simeq 15 \text{ g cm}^{-2}$ .

For typical interstellar grain opacities ( $\kappa_{0.7\mu} \simeq 100 \text{ cm}^2 \text{ g}^{-1}$  and  $\kappa_{2\mu} \simeq 5 \text{ cm}^2 \text{ g}^{-1}$ , Draine & Lee 1984) we thus derive  $\tau_\lambda \gg 1$  at both visual and near-IR wavelengths, consistent with the suggested interpretation of AA Tau’s light curve. Reducing the rough estimate of  $\Delta r$  above by a factor of 10 would still lead to optically thick material.

In summary, variable circumstellar extinction appears to provide a plausible explanation for AA Tau’s light curve. Dust is expected to exist at the distance required to account for the photometric period and is most likely optically thick thus producing recurrent occultations of the stellar photosphere. In the next section, we discuss the origin of the non-axisymmetric inner disk wall that might produce these occultations and discuss the various aspects of AA Tau’s variability in the framework of a geometrical model for its accretion region.

## 5. Discussion

Although we cannot firmly rule out any of the interpretations discussed in the previous section, variable circumstellar extinction appears to be the most likely explanation of

AA Tau’s variability at the time we observed it. If indeed quasi-periodic occultations of the stellar photosphere occur due to circumstellar material orbiting the star at a few stellar radii, this provides an opportunity to constrain the geometry of the accretion zone in a T Tauri star using an approach somewhat similar to the eclipse-imaging techniques developed for other classes of objects such as cataclysmic variables. We therefore investigate this hypothesis further in this section, present a tentative model for what might be the structure of the star-disk interaction zone in AA Tau’s system and discuss its implications for current models of magnetospheric accretion in T Tauri stars.

### 5.1. A geometrical model for the occultation scenario

Various lines of evidence suggest that T Tauri stars accrete material from their circumstellar disk through the stellar magnetosphere (Hartmann 1998). In the framework of the occultation model for AA Tau, the non-axisymmetric inner disk wall may be naturally understood as resulting from the interaction between the inner accretion disk and a *tilted* stellar dipole. A stellar dipole tilted with respect to the stellar rotational axis is expected to break the axisymmetry of the magnetospheric accretion flow as material at the inner disk edge will be more easily loaded onto the shorter field lines connecting the disk to the star (Mahdavi & Kenyon 1998).

**Table 4.** Magnetospheric accretion model: parameters and results

Stellar parameters	
Stellar inclination:	$i = 75^\circ$
Stellar mass:	$M_\star = 0.8M_\odot$
Stellar radius:	$R_\star = 1.85R_\odot$
Stellar luminosity:	$L_\star = 0.8L_\odot$
Rotational period:	$P_{rot} = 8.4 \text{ d}$
Model parameters	
Inner disk wall located at:	$r_c = 8.8R_\star$
Maximum vertical extent:	$h_m = 0.3r_c$
Azimuthal structure:	$h(\phi) = h_m \left  \cos \frac{(\phi - \phi_0)}{2} \right $
Radial extent:	$\Delta r \ll r_c$
Inclination of the stellar dipole:	$\beta = 52^\circ$
Results	
Keplerian period at the inner disk edge:	$P_{kep} = 8.5d$
Visible fraction of the photosphere:	100% at $\phi = 0$ 23% at $\phi = 0.5$
Spots latitude (spots center):	$\pm 37^\circ$
Spots angular radius (non circular):	$\simeq 15^\circ$
Spots area (N+S) / $4\pi R_\star^2$	3.4%
Projected area of the hot spots / $\pi R_\star^2$ :	N: 6.3% at $\phi = 0.5$ S: 4.2% at $\phi = 0$
Visible area of the hot spots / $\pi R_\star^2$ :	N: 1.5% at $\phi = 0.5$ S: 4.2% at $\phi = 0$

Even though the detailed physics of the interaction has still to be elucidated, it may be expected that the inner disk will thus be distorted by the non-axisymmetric magnetosphere and assume a shape resembling that of the inner disk wall advocated above to account for AA Tau’s light curve, as schematically illustrated in Fig. 10. The disk wall would then be located at the so-called magnetospheric radius,  $r_m$ , at which magnetic forces start to significantly affect the dynamics of the accretion flow.

Assuming that the development of the disk wall is a consequence of the interaction between the inner accretion disk and a tilted stellar dipole, we investigate whether such a model can account for the observations reported here. The geometric model relies on the following assumptions:

- AA Tau possesses a large-scale dipolar magnetic field whose axis makes an angle  $\beta$  with the spin axis.
- the dipolar field truncates the disk at a distance  $r_m$ . From this radius inwards, the accretion flow is directed onto the star along the magnetic field lines.
- as the free-falling material hits the stellar surface, an accretion shock develops at the foot of magnetic structure thus forming a bright accretion ring around each magnetic pole (see Mahdavi & Kenyon 1998).

Two parameters,  $r_m$  and  $\beta$ , entirely define the geometry of the dipole as well as the location and the shape the hot accretion rings at the stellar surface. As argued above, we assume  $r_m = r_c = 8.8R_\star$ . The tilt angle of the dipole with respect to the spin axis,  $\beta$ , is not directly constrained by our data but can

be estimated from the redshifted absorption features seen in the emission line profiles of AA Tau. These absorptions are thought to result from material being accreted at free-fall velocity onto the stellar surface. Edwards et al. (1994) measured maximum projected radial velocities ranging from about  $300\text{kms}^{-1}$  to  $350\text{kms}^{-1}$  at the red edge of AA Tau’s Balmer and NaD absorptions. For a truncation radius of  $8.8R_\star$ , the free-fall velocity of accreted material is

$$v_{ff} = \{2GM_\star/R_\star \cdot (1 - R_\star/r_m)\}^{1/2} \simeq 380\text{kms}^{-1}$$

with  $M_\star = 0.8M_\odot$  and  $R_\star = 1.85R_\odot$ , which leads to  $\cos i_m \simeq 0.92$ , where  $i_m$  is the inclination of the magnetic axis on the line of sight. We thus derive  $\beta = i_\star - i_m \simeq 52^\circ$  as a rough estimate of the dipole inclination.

The appearance of the system at several rotational phases is shown in Fig. 10 and described more quantitatively in Table 4. In this geometry, two hot accretion shocks develop at the stellar surface, one on the “northern” hemisphere which is partly occulted together with the photosphere and an opposite one on the “southern” hemisphere which is fully visible at the opposite phase.

As illustrated in Fig. 9, this model reasonably reproduces the overall light variations of AA Tau. The midterm color behaviour of AA Tau can be qualitatively understood in this framework as well. The blue excess is expected to arise from the hot accretion rings at the footpoint of the magnetic structure. For simplicity, we assume that the blue excess emitting region is the area enclosed by the accretion rings, i.e., we consider them as bright spots. This assumption does not affect our conclusions since the relative visibility of the accretion shocks whether considered as uniformly bright spots or rings is about the same. In particular, the model predicts that only about 25% of the area of the northern spot is visible at the center of the occultations and a similar result would be obtained assuming a ring (see Fig. 10).

The blue excess luminosity is then expected to vary with time, as the *effective* area of the hot spots is modulated by rotation and occultations. The model predicts that the effective (i.e., unocculted) projected area of the northern and southern spots is 1.5% and 4.2% of the stellar hemisphere at minimum and maximum brightness, respectively (Table 4). Hence, the blue excess flux is expected to be larger at maximum brightness as observed. Furthermore, the color of the system as well as the amount of veiling is expected to change as the spots *fractional* area varies. Defining the fractional spot area as  $R_A = A_{spot}^{eff}/A_\star^{eff}$ , the system will be bluer and exhibit more veiling as this ratio increases. The model predicts  $R_A = 0.06$  at the center of the occultation and  $R_A = 0.04$  at the opposite phase, which qualitatively accounts for the slightly bluer colors and stronger veiling of the system during the occultations. Admittedly, these estimates are sensitive to the values derived above for the stellar and dipole inclinations. Nevertheless, they serve to illustrate that the midterm brightness, color and veiling variations observed for AA Tau can be at least qualitatively understood in the framework of the model outlined here.

Another component of AA Tau’s photometric variations is the short-term brightening events that are primarily observed

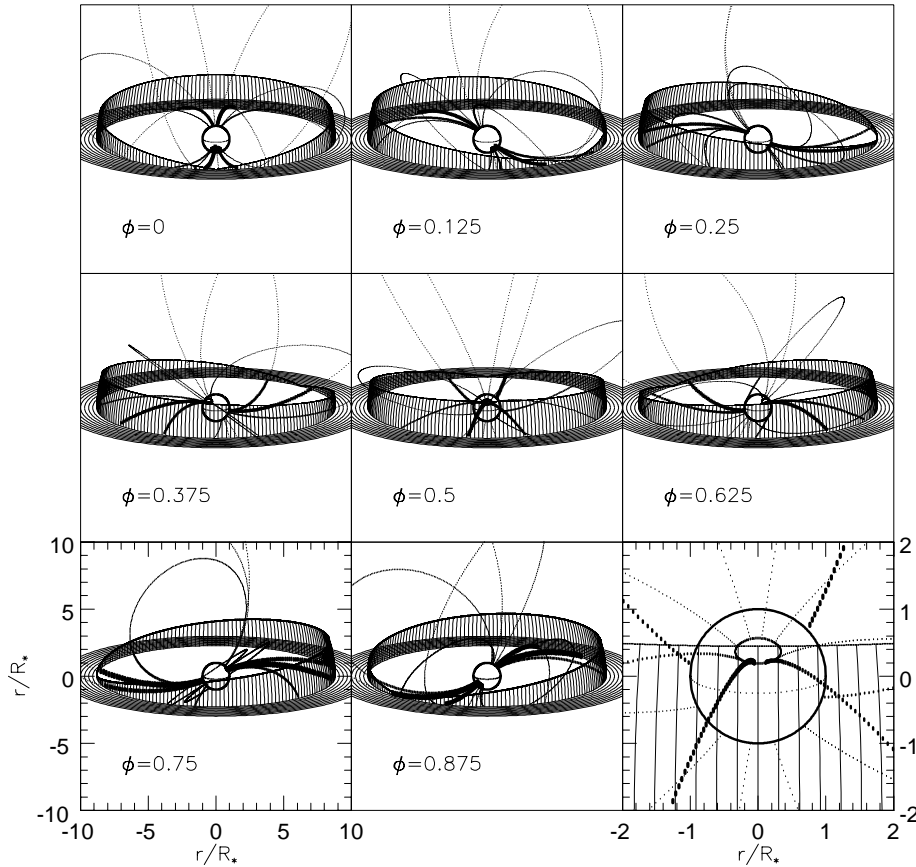


**Fig. 10.** The appearance of the AA Tau system at several observational phases. The system consists of a late-type star with an inclined dipolar magnetic field ( $\beta = 52^\circ$ ) that truncates the disk at a distance of  $8.8R_*$  from the star's center. The dynamical interaction between the magnetic field and the disk leads to the development of a “disk wall” at the truncation radius that produces recurrent occultations at around  $\phi = 0.5$ . For clarity, only the upper part of the disk thickening above the disk's midplane is shown. The whole system is centrosymmetric relative to the star center. Two opposite hot spots develop at the footpoints of the dipole where the kinetic energy of the material accreted along field lines is dissipated in a shock. The thickness of field lines qualitatively illustrates the density of accreted material: more material is accreted along the shorter field lines, which results in an azimuthally varying height for the disk wall. The lower-right panel is a close-up view of the system at  $\phi = 0.5$ .

within occultations and during which the system becomes suddenly bluer. The most conspicuous of these events observed around day 37.6 and 46.8 have a typical duration of about 0.5 days and an amplitude of nearly 1 magnitude in the B-band (Fig. 9). That these events are preferentially observed during the occultations might merely be a contrast effect. However, Fig. 6 shows that the flux in the  $H_\beta$  line tends to correlate with the transient brightening episodes and that the intranight scatter of the  $H_\beta$  line flux appears systematically larger during the occultations. Since the line flux is not affected by contrast effects, this does suggest that the transient episodes primarily occur in the faint state. If ascribed to non-steady accretion onto the star, these episodes would be expected to be observed at all photometric phases and in particular when the system is bright as one of the accretion shocks is in view and the blue excess is at its maximum. It thus appears more likely that these transient events result from small scale inhomogeneities of reduced optical thickness in the occulting material. In support of this interpretation we note that the time it takes for any part of the occulting material to transit the stellar photosphere is of the order of:

$$\Delta t \simeq \frac{2R_*}{r_c} \frac{P_{kep}}{2\pi} \simeq 0.3 d$$

which is roughly similar to the timescale of the brightening episodes. Because the accretion shock is much hotter than the photosphere, a moderate change in the occulted area of the bright

spot will produce a significant brightening and blueing of the system.

The observed correlation between the continuum flux and the  $H_\alpha$  line flux from day 38 to 48 (Fig. 6) suggests that the line emitting region is partly occulted at the same time as is the photosphere, albeit to a lesser degree since the  $H_\alpha$  equivalent width increases at minimum brightness. On the other hand, the  $H_\alpha$  line flux does not respond to transient brightening episodes: during these episodes, the  $H_\alpha$  flux scatter does not exceed that observed at any other phase. Altogether, this suggests that the  $H_\alpha$  emitting volume is much more extended than the bright spot and yet at least partly restricted to within the occulted volume. This is consistent with the  $H_\alpha$  line being formed in the bulk of the magnetospheric funnel flow. In contrast, the  $H_\beta$  line flux seems to strongly react to the transient brightening episodes, closely mimicking the variations of the nearby continuum flux. If these brightening events are due to small scale inhomogeneities in the occulting material, this suggests that the  $H_\beta$  line forms in a restricted volume closely connected to the hot surface spot.

The partial occultation of the line emitting regions is probably not the only source of line flux variability since the observed correlation between line and continuum fluxes appears to break down after day 48. Moreover, on day 44 the  $H_\beta$  line flux becomes suddenly much larger while the system is still in the bright state. This may point to an additional, intrinsic source of variability for the line fluxes possibly related to non-steady accretion on a timescale of days.

In the framework of the occultation model, the higher level of linear polarization observed at minimum light simply results from the depressed photospheric flux relative to scattered light. Most likely, polarized light primarily arises from stellar photons being scattered back to the observer by the disk wall as it is directly illuminated by the bright accretion shock and subtends a significant solid angle as viewed from the star (see Fig. 10). The observed variations of the polarization angle can then be qualitatively understood as reflecting the changing orientation of the scattering plane as seen from the observer as the system rotates (Bastien 1981, Stassun & Wood 1999). For the same reasons, the irradiated disk wall may be expected to significantly contribute to the near-IR excess flux. At maximum brightness, the observer sees the illuminated part of the disk wall that lies above the disk midplane while at minimum light it is the part lying below the disk midplane that is seen (see Fig. 10). Therefore, the near-IR excess flux is not expected to vary much during the photometric cycle.

In summary, the geometrical model investigated here on the basis of the current paradigm of magnetic accretion in T Tauri stars appears to qualitatively account for AA Tau's spectrophotometric and polarimetric variability. This supports a large-scale, tilted stellar dipole as being the dominant magnetic component that interacts with the inner accretion disk in T Tauri stars.

## 5.2. Implications for magnetospheric accretion models

In most magnetospheric accretion models developed so far to account for the low rotation rates of T Tauri stars, the magnetospheric radius  $r_m$  at which the stellar magnetic field truncates the disks lies in the vicinity of the corotation radius  $r_{co}$ , i.e., the radius at which the keplerian angular velocity in the disk is equal to the star's angular velocity (Shu et al. 1994, Paatz & Camenzind 1996, King & Regev 1994, Ferreira 1999). A rotational equilibrium results in less than a million years and maintains the star at a roughly constant angular velocity as long as it accretes from the disk (Armitage & Clarke 1996).

The data reported here for AA Tau provides a direct estimate of the relative location of the disk's truncation and corotation radii. The corotation radius is defined as  $r_{co} = (GM_\star)^{1/3} (P_{rot}/2\pi)^{2/3}$  where  $P_{rot}$  is the star's rotational period. Vrba et al. (1989) first reported a photometric period of 8.2d in a light curve of AA Tau obtained in 1984 and ascribed it to the star's rotational period. The question immediately arises whether the photometric modulation at that time was due to surface spots, in which case the photometric period is the star's rotational period, or whether it was due to quasi-periodic occultations, as reported here. Even though Vrba et al.'s (1989) light curve is sparsely sampled, with only about 30 measurements over 20 days, it shares striking similarities with the one we obtained 11 years later: the photometric amplitudes are comparable, there are no significant color changes in the BVRI bands, and the overall shape of the light curve is reminiscent of the one obtained here. It is therefore most likely that at the time Vrba et al. (1989) observed it, AA Tau's photometric variations were dominated

by the occultation phenomenon and not by spot modulation. It is interesting to note that Vrba et al. (1989) also obtained measurements in the U-band which exhibit much lower photometric amplitudes than in the BVRI bands, amounting to approximately 0.5 and 1.0 magnitudes, respectively. This is actually expected in the occultation model since the U-band flux is dominated by the hot spots at all photometric phases and not by the stellar photosphere. During the occultations, transient brightening episodes are much stronger at short wavelengths and will therefore tend to reduce the average amplitude of variability in the U-band.

Vrba et al. (1993) monitored again the photometric variations of AA Tau in 1985. The light curve was then quite different: the photometric amplitudes were somewhat reduced compared to the 1984 light curve, amounting to 0.8 mag in the V-band and, more importantly, strong color variations were observed with photometric amplitudes decreasing from 1.1 mag in the U-band to 0.6 mag in the I-band. This behaviour is typical of a modulation of the system's luminosity by hot spots with a temperature of about 500–1500 K hotter than the photosphere. Vrba et al. (1993) found a photometric period of 4.2d in this light curve which is half of the previously reported period and interpreted it as indicating the presence of two opposite spots at the stellar surface. This result is consistent with the geometric model presented here since when the light curve is dominated by spots modulation the photometric wave is expected to be double-peaked within a full rotational cycle as the opposite spots on the stellar surface come into view successively. The rotational period of AA Tau thus derived amounts to  $8.4 \pm 0.1$ d, which is also consistent with AA Tau's projected rotational velocity of  $v \sin i = 11 \text{ km s}^{-1}$  if the system is seen nearly edge-on.

This estimate of AA Tau's rotational period yields  $r_{co} = 8.7 \pm 0.1 R_\star$ . We thus find that the disk inner edge lies close to the corotation radius,  $r_m \simeq r_{co}$ . This provides strong support to the idea that the stellar magnetic field becomes dynamically important in controlling the accretion flow in the disk in the vicinity of the corotation radius. The near coincidence of the magnetospheric and corotation radii in AA Tau's system could in principle also account for AA Tau's rotational period in the framework of the disk regulation hypothesis. The 8.4d period lies close to the mode of the narrow distribution of rotational periods of accreting T Tauri stars in the Taurus cloud (Bouvier et al. 1993, Edwards et al. 1993) which suggests that it is in a state of rotational equilibrium. However, the relevance of such a regulation mechanism in accreting T Tauri stars has recently been questioned by Stassun et al. (1999) who did not find much supporting evidence for it from the study of rotation in a large sample of T Tauri stars in and around the Orion nebula.

With such a large inner disk hole, one could expect AA Tau's spectral energy distribution (SED) to exhibit a flux deficiency around  $2 \mu\text{m}$  since in non-truncated disks the near-IR excess flux occurs predominantly in the disk inner regions located at a few stellar radii from the photosphere (Meyer et al. 1997). Yet, Basri & Bertout (1989) obtained a reasonably good fit to AA Tau's SED from UV to near-IR wavelengths without having to invoke an inner disk hole. It remains unclear, however, whether

large disk holes would necessarily produce a clear signature in the near-IR. An illustrative counter-example is the case of DQ Tau, an accreting T Tauri spectroscopic binary with an orbital period of 15.8 days (Mathieu et al. 1997). At periastron, the two stars are only about  $8R_*$  apart, which undoubtedly leads to the destruction of the inner disk and possibly to the direct interaction of the stellar magnetospheres (Basri et al. 1997). Yet, DQ Tau's SED is quite typical of that of most accreting T Tauri stars, resembling a power-law from 1 to  $60 \mu\text{m}$  and exhibiting a strong excess at 2.2 and  $10 \mu\text{m}$ . Mathieu et al. (1997) showed that very little material is actually required to produce these excesses: they derived that a total mass of  $5 \cdot 10^{-10} M_\odot$  of warm optically thin dust in the disk hole is enough to account for DQ Tau's near-IR excesses. Hence, the moderate near-IR excess of AA Tau does not rule out the model outlined here, provided there is a minimum amount of warm optically thin dust close to the star. A distinctive signature of such a dusty component would be a strong silicate emission feature at  $10 \mu\text{m}$ . Unfortunately, spectroscopic observations of AA Tau at this wavelength do not appear to exist yet.

### 5.3. AA Tau's magnetic field: strength and topology

The determination of the truncation radius in AA Tau's disk provides an order of magnitude estimate of the strength of the stellar magnetic field. Equating the ram pressure of the gas in the disk to the magnetic pressure of the dipole at the truncation radius (Elsner & Lamb 1977) leads to:

$$r_m^{7/2} = B_*^2 R_*^6 (GM_*)^{-1/2} \dot{M}_{acc}^{-1}$$

where  $B_*$  is the magnetic field strength at the stellar surface and  $\dot{M}_{acc}$  is the mass-accretion rate in the inner disk.

An estimate of the mass accretion rate can be derived from the luminosity of the blue excess assumed to arise in the accretion shocks:

$$L_{spots} = A_{spots} \cdot \sigma T_{spot}^4 \simeq \frac{1}{2} \frac{GM_* \dot{M}_{acc}}{R_*}$$

where  $A_{spots}$  is the total area covered by the 2 opposite spots at the stellar surface (see Table 4) and we have neglected the term  $(1 - R_*/r_m) \simeq 1$  for the accretion luminosity.

The spot temperature is derived by assuming that the spots and the photosphere radiate like black-bodies at temperatures  $T_{spot}$  and  $T_{eff}$ , respectively. The excess flux measured in the B-band ( $\lambda = 0.44 \mu\text{m}$ ) at maximum brightness is then:

$$F_{spot}^\lambda = \frac{A_{spot(S)}^{eff}}{d^2} \cdot 10^{0.4A_\lambda} \cdot \pi B_\lambda(T_{spot})$$

where  $A_{spot(S)}^{eff}$  is the projected surface of the southern spot at maximum visibility (see Table 4),  $A_B = 1.33A_V = 1.2 \text{ mag}$  (see Appendix), and  $d = 140 \text{ pc}$ . From AA Tau's SED we measure  $F_{spot}^\lambda = 4.5 \cdot 10^{-15} \text{ erg cm}^{-2} \text{ s}^{-1} \text{ \AA}^{-1}$  which yields  $T_{spot} \simeq 5000 \text{ K}$ . This estimate is similar to the spot temperature deduced by Vrba et al. (1993) by fitting the amplitude of photometric variability from 0.44 to  $0.79 \mu\text{m}$ . The actual spot

temperature may actually be higher if we overestimated the surface of the accretion shocks by assuming that they are uniformly bright spots instead of rings. Moreover, if the blue excess emitting region is partially optically thin in the Paschen continuum (Bertout & Basri 1989, Valenti et al. 1993), the above estimate is merely a lower limit to the actual spot temperature.

The luminosity of the spots is thus found to be  $L_{spots} = 6.5 \cdot 10^{-2} L_\odot = 0.08 L_*$ , which leads to  $\dot{M}_{acc} \simeq 10^{-8} M_\odot \text{ yr}^{-1}$ , with  $M_* = 0.8 M_\odot$  and  $R_* = 1.85 R_\odot$ . Mass accretion rates ranging from  $3 \cdot 10^{-9}$  to  $5 \cdot 10^{-8} M_\odot \text{ yr}^{-1}$  have been derived for AA Tau at different epochs and by different methods by Bertout & Basri (1989), Gullbring et al. (1998), Hartigan et al. (1991), and Valenti et al. (1993). We therefore adopt a range of plausible mass accretion rates from  $10^{-9}$  to  $10^{-8} M_\odot \text{ yr}^{-1}$  for AA Tau which, with  $r_m = 8.8 R_*$ , leads to  $B_* \simeq 0.5\text{--}1.5 \text{ kG}$  at the stellar surface. Although no Zeeman measurements exist for AA Tau, surface magnetic fields in this range have been recently reported for several classical T Tauri stars (Guenther et al. 1999, Johns-Krull et al. 1999).

There are a number of clues in favour of a large-scale magnetic dipole in AA Tau. We already mentioned a few: the tilted dipole hypothesis naturally leads to the development and azimuthal structure of the disk's wall and to the opposite location of the hot spots on the stellar surface which are required to explain the observations. A single or a few huge magnetic loops interacting with the disk would certainly lead to quite different light curves. Another indirect argument in favor of a large-scale dipole is the apparent stability of the phenomenon. AA Tau's photometric period was detected by Vrba et al. (1989, 1993) in light curves spanning 149 days in 1984 and 174 days in 1985, i.e., 18 and 20 photometric cycles, respectively. Similarly, the light-curve reported here suggests recurrent occultations over at least 4 keplerian periods, even though the detailed shape of the occultations does vary from one cycle to the next. The overall structure thus appears stable on a timescale of at least several months, and perhaps many years as suggested by the resemblance between Vrba et al.'s 1984 light curve and ours obtained more than 10 years later. On at least one occasion, however, the occultation phenomenon had apparently vanished (in Vrba et al.'s 1985 light curve) which suggests long-term variations of the structure which could conceivably be related to a magnetic dynamo cycle. Alternatively, if the mass accretion rate in the inner disk does not match that on the star, one may speculate that material piles up at the magnetospheric radius until it is eventually accreted onto the star, thus leading to long term variations of the inner disk structure.

The data reported here thus supports the existence of a relatively strong, large-scale dipolar field in AA Tau, which is the dynamically dominant magnetic structure at the disk's truncation radius. This does not exclude the existence of other components in AA Tau's magnetic field. Safier (1998) summarized the observational evidence for small-scale and rapidly varying magnetic structures in T Tauri stars which mainly comes from the ubiquitous variability of these objects in the X-ray domain (Montmerle & Casanova 1996). AA Tau was observed twice at X-ray frequencies by Walter & Kuhi (1984) with the Einstein

satellite. It was detected as a strong X-ray emitter in March 1980, but remained undetected about a year later in February 1981. The X-ray “disappearance of AA Tau” (Walter & Kuhi 1984) was tentatively interpreted as a temporary occultation of the X-ray emitting region due to enhanced absorption column density on the line of sight. This interpretation is supported by the model outlined here. Walter & Kuhi (1984) obtained a low-resolution optical spectrum only 36 hours before AA Tau’s X-ray disappearance, and another 12 days later. The first spectrum exhibits much stronger Balmer line emission and a much bluer continuum slope than the second one. Compared to the observations reported here, which indicate that Balmer line emission increases during occultations, this suggests that AA Tau was indeed occulted at the epoch of its X-ray disappearance. Altogether, and in spite of the almost 2 decades elapsed between Walter & Kuhi’s (1984) study and ours, this is consistent with X-ray emission arising from a region close to the stellar surface which undergoes occultations at the same time as the photosphere.

In summary, the global view of AA Tau’s magnetic field that emerges is a combination of a stable large-scale dipole which interacts with the inner accretion disk and rapidly varying, small-scale magnetic structures extending at most a few stellar radii from the photosphere where X-ray emission arises. Overall, this structure is reminiscent of the topology and temporal behaviour of the Sun’s magnetic field.

#### 5.4. Alternative models: accretion or wind curtains?

We have argued that recurrent occultations of AA Tau’s photosphere are produced by an optically thick dusty wall located near the corotation radius in the disk. From the geometrical model above, we find  $h/r \simeq 0.3$  at the truncation radius as compared to  $h/r \simeq 10^{-2} - 10^{-1}$  in classical  $\alpha$ -disk models. The thickening of the inner disk is expected to result from the dynamical interaction between the disk and the stellar magnetosphere (Agapitou et al. 1997, Miller & Stone 1997, Campbell 1998).

There are, however, at least two conceivable alternatives for the source of the occultations. One is to assume that the funnel accretion flow in the magnetosphere is itself dense enough at least at some azimuths to be optically thick in the continuum: such an accretion “curtain” (Ferrario 1997) could periodically occult the photosphere as the system rotates. Another source for the occultations could be a wind “curtain” since the wind is thought to arise at least partly from the truncation radius.

These alternatives require that the gas in the accretion or wind “curtains” be optically thick in the continuum in order to produce grey occultations and relatively cold so that it does not contribute significantly to the continuum emission, as demanded by AA Tau’s weak veiling. An order of magnitude estimate of the density of the accretion flow can be derived from the mass accretion rate and the geometry of the system, and it is likely that the wind density will be lower than that of the accretion

flow. The mass-accretion rate onto the star is of order:

$$\dot{M}_{acc} \simeq A_{spots} \cdot n_H \cdot m_H \cdot V_{ff}$$

where  $n_H$  is the gas density and  $V_{ff}$  the free fall velocity. This leads to  $n_H \simeq 10^{12} \text{ cm}^{-3}$  for  $\dot{M}_{acc} = 10^{-8} M_{\odot} \text{ yr}^{-1}$ . Assuming that the depth of the accretion flow on the line of sight is of order  $0.1 r_m \simeq R_*$ , the resulting hydrogen column density is  $N_H \simeq 10^{23} \text{ cm}^{-2}$ . We computed rough estimates of the gas optical depth in the Paschen continuum from free-free, free-bound and  $\text{H}^-$  opacities for various arbitrary temperatures and ionisation fractions since the temperature structure in funnel flows is still uncertain (Martin 1997, Hartmann et al. 1994, Calvet & Gullbring 1998). All these estimates suggest that the gas is totally transparent to stellar photons in the continuum (see also Lamzin 1995, Königl 1991). Similarly, Thomson scattering of stellar photons by free electrons would require an electron column density of order of  $\simeq 10^{24} \text{ cm}^{-2}$  to start to produce observable effects. Hence, unless we have severely underestimated the gas density in the magnetosphere or in the wind, or the thickness of these flows on the line of sight, curtain flows are unlikely to be the source of the occultations. Proper computations of statistical equilibrium and radiative transfer are beyond the scope of this paper but should nevertheless be run in order to further investigate these alternatives.

## 6. Conclusion

From a high temporal resolution monitoring of AA Tau’s photometric variations over several rotational periods, we have found that its light curve exhibits specific signatures that we interpret as due to recurrent occultations of the stellar surface by opaque circumstellar material. The obscuring material is tentatively identified with an inner disk “wall”, i.e., a non-axisymmetric thickening of the disk inner edge at the corotation radius. A model in which a tilted stellar dipole disrupts the accretion disk at the corotation radius consistently accounts for the photometric, spectroscopic and polarimetric variations of AA Tau at this epoch.

These results thus support the paradigm of magnetospheric accretion in T Tauri stars and suggest that the dominant magnetic structure that interacts with the inner disk is a large-scale dipole tilted with respect to the rotational axis. In addition, the disk’s inner edge as defined by the magnetospheric radius is found to lie at or close to the corotation radius, consistent with the idea that T Tauri stars rotation rates are regulated by the magnetospheric accretion process.

AA Tau’s average spectrum and spectral energy distribution are prototypical of the whole class of CTTS. It is probably only because the system is seen close to edge-on that its light curve is qualitatively different from those of most other accreting T Tauri stars seen at more moderate inclinations. Therefore, the constraints derived on the structure of its accretion region might apply as well to other classical T Tauri stars.

AA Tau and perhaps another couple of T Tauri stars that appear to exhibit a similar photometric behaviour provide an opportunity to apply zeroth-order eclipse-imaging techniques to

constrain the structure and the physical conditions of the accretion zone in classical T Tauri stars. From multi-wavelength photometry and low-resolution spectroscopy, we have attempted here to derive its overall structure. In the future, simultaneous monitoring of the variations of emission line profiles at high spectral resolution will bring further insight into the location and physical properties of the line emitting regions as well as on the connection between the accretion and ejection processes in T Tauri stars.

*Acknowledgements.* It is a pleasure to thank C. Bertout, S. Cabrit, A. Chalabaev, J. Ferreira, M. Forestini and C. Terquem for useful discussions. We thank R. Mathieu for communicating unpublished results on AA Tau's radial velocity variations and the referee, Dr. W. Herbst, whose comments greatly helped to improve the presentation of the results. Support for polarimetric studies of stars at Steward Observatory is provided to G.S. through NSF grant AST 97-30792. L.C. was supported by a CONACYT grant G28586E.

## Appendix A: stellar parameters

We reexamine the stellar parameters of AA Tau in the light of the above results. The bright (unocculted) state of AA Tau is used to estimate its luminosity after correcting for visual absorption on the line of sight. At maximum luminosity,  $(V - R)_c = 0.96$ , which leads to a color excess  $E(V-R)_c = 0.12$ , assuming a spectral type K7 and intrinsic Cousins colors for dwarfs listed by Kenyon & Hartmann (1995). This yields  $A_v = 0.78$  mag. This estimate of  $A_v$  should not be much affected by AA Tau's weak veiling (we measured  $r = 0.15 \pm 0.05$  on J.D. 50.55 and 50.60), nor by scattered light, which both primarily affect colors at shorter wavelengths.

With  $V=12.5$  in the bright state, and a bolometric correction  $B.C. = -0.87 \pm 0.05$  for a K7 dwarf (Kenyon & Hartmann 1995), we then obtain  $L_*/L_\odot = 0.8 \pm 0.1$ . Combining this estimate with  $T_{eff} = 4030 \pm 30$  K for a K7 dwarf, one gets  $R_*/R_\odot = 1.85 \pm 0.15$ . From Baraffe et al. (1998) evolutionary models, we deduce a stellar mass of  $0.85M_\odot$  (resp.  $0.75M_\odot$ ) and an age of 2.2 Myr (resp. 1.6 Myr) for a mixing-length parameter of 1.5 (resp. 1.9). In both cases, the star is fully convective.

From the high-resolution spectra, we obtain  $v \sin i = 11 \pm 1.5$   $\text{kms}^{-1}$  for AA Tau's projected rotational velocity, consistent with Hartmann & Stauffer's (1989) measurement of  $v \sin i = 11.4 \text{kms}^{-1}$ . From this and the estimate of the stellar radius above, we derive  $P_{rot}/\sin i = 2\pi R_*/v \sin i = 8.5d$ . Taking into account  $1\sigma$  uncertainties on the stellar radius,  $v \sin i$  and rotational period ( $8.4 \pm 0.1$  d, Vrba et al. 1993), we thus derive a lower limit of  $\sin i \geq 0.8$  for the stellar inclination. Based on the evidence that the system is seen at a high inclination (see 4.3), we adopt  $i = 75^\circ$  in the geometric model presented in this paper.

## References

Agapitou V., Papaloizou J.C.B., Terquem C., 1997, MNRAS 292, 631  
 Armitage P.J., Clarke C.J., 1996, MNRAS 280, 458  
 Baraffe I., Chabrier G., Allard F., Hauschild P.H., 1998, A&A 337, 4003

Baranne A., Queloz D., Mayor M., et al., 1996, A&AS 119, 373  
 Basri G., Bertout C., 1989, ApJ 341, 340  
 Basri G., Johns-Krull C.M., Mathieu R., 1997, AJ 114, 781  
 Bastien P., 1981, A&A 94, 294  
 Bertout C., 1989, ARA&A 27, 351  
 Bertout C., Basri G., Bouvier J., 1988, ApJ 330, 350  
 Bouvier J., Cabrit S., Fernandez M., Martín E.L., Matthews J.M., 1993, A&A 272, 176  
 Bouvier J., Covino E., Kovo O., et al., 1995, A&A 299, 89  
 Calvet N., 1997, In: Reipurth B., Bertout C. (eds.) Herbig-Haro Flows and the Birth of Stars. IAU Symposium No. 182, Kluwer Academic Publishers, p. 417  
 Calvet N., Gullbring E., 1998, ApJ 509, 802  
 Campbell C.G., 1998, MNRAS 301, 754  
 Choi P.I., Herbst W., 1996, AJ 111, 283  
 Claret A., 1998, A&A 335, 647  
 Collier Cameron A., Campbell C.G., 1993, A&A 274, 309  
 Cruz-González I., Carrasco L., Ruiz E., et al., 1994, In: Crawford D.L., Craine E.R. (eds.) Instrumentation in Astronomy VIII, Proc. SPIE 2198, 774  
 Dorren J.D., 1987, ApJ 320, 756  
 Draine B.T., Lee H.M., 1984, ApJ 285, 89  
 Dworetzky M.M., 1983, MNRAS 203, 917  
 Eaton N.L., Herbst W., 1995, AJ 110, 2369  
 Edwards S., 1997, In: Reipurth B., Bertout C. (eds.) Herbig-Haro Flows and the Birth of Stars. IAU Symposium No. 182, Kluwer Academic Publishers, p. 433  
 Edwards S., Strom S.E., Hartigan P., et al., 1993, AJ 106, 372  
 Edwards S., Hartigan P., Ghandour L., Andrulis C., 1994, AJ 108, 1056  
 Elsner R.F., Lamb F.K., 1977, ApJ 215, 897  
 Ferrario L., 1997, In: Wickramasinghe D.T., Bicknell G.V., Ferrario L. (eds.) Accretion Phenomena and Related Outflows. IAU Colloquium 163. ASP Conference Series Vol. 121, p. 403  
 Ferreira J., 1997, A&A 319, 340  
 Ferreira J., 1999, A&A, in press  
 Gahm G.F., Fischerström C., Liseau R., Lindroos K.P., 1989, A&A 211, 115  
 Guenther E.W., Lehmann H., Emerson J.P., Staude J., 1999, A&A 341, 768  
 Gullbring E., Hartmann L., Briceño C., Calvet N., 1998, ApJ 492, 323  
 Hartigan P., Edwards S., Ghandour L., 1995, ApJ 452, 736  
 Hartigan P., Hartmann L., Kenyon S., Strom S.E., Skrutskie M.F., 1990, ApJ 354, L25  
 Hartigan P., Kenyon S.J., Hartmann L., et al., 1991, ApJ 382, 617  
 Hartmann L., 1998, Accretion Process in Star Formation. Cambridge Astrophys. Ser., Vol.32  
 Hartmann L., Stauffer J.R., 1989, AJ 97, 873  
 Hartmann L., Hewett R., Calvet N., 1994, ApJ 426, 669  
 Hartmann L., Hewett R., Stahler S., Mathieu R.D., 1986, ApJ 309, 275  
 Herbst W., Herbst D.K., Grossman E.J., 1994, AJ 108, 1906  
 Hirth G.A., Mundt R., Solf J., 1997, A&AS 126, 437  
 Johns-Krull C., Valenti J.A., Hatzes A.P., Kanaan A., 1999, ApJ 501, L41  
 Kenyon S.J., Hartmann L., 1995, ApJS 101, 117  
 King A.R., Regev O., 1994, MNRAS 268, L69  
 Königl A., 1991, ApJ 370, L39  
 Kwan J., 1997, ApJ 489, 284  
 Lamzin S.A., 1995, A&A 295, L20  
 Landolt A.U., 1983, AJ 88, 439  
 Mahdavi A., Kenyon S.J., 1998, ApJ 497, 342

- Martin S.C., 1997, In: Reipurth B., Bertout C. (eds.) *Herbig-Haro Flows and the Birth of Stars*. IAU Symposium No. 182, Kluwer Academic Publishers, p. 455
- Mathieu R.D., Stassun K., Basri G., et al., 1997, *AJ* 113, 1841
- Meyer M.R., Calvet N., Hillenbrand L.A., 1997, *AJ* 114, 288
- Miller K.A., Stone J.M., 1997, *ApJ* 489, 890
- Montmerle T., Casanova S., 1996, In: Uchida Y., Kosugi T., Hudson H.S. (eds.) *Magnetodynamic phenomena in the solar atmosphere*. IAU Coll. 153, Kluwer Academic Publishers, Dordrecht, p. 247
- Muzerolle J., Calvet N., Hartmann L., 1998, *ApJ* 492, 743
- Paatz G., Camenzind M., 1996, *A&A* 308, 77
- Papaloizou J.C.B., Terquem C., 1999, *ApJ*, in press
- Popham R., 1996, *ApJ* 467, 749
- Roberts D.H., Lehar J., Dreher J.W., 1987, *AJ* 93, 968
- Safier P., 1998, *ApJ* 494, 336
- Schmidt G.D., Stockman H.S., Smith P.S., 1992, *ApJ* 398, L57
- Shevchenko V.S., Grankin K.N., Ibragimov M.A., et al., 1991, *IBVS* 3652, 1
- Shu F., Najita J., Ostriker E., et al., 1994, *ApJ* 429, 781
- Skrutskie M.F., Meyer M.R., Whalen D., Hamilton C., 1996, *AJ* 112, 2168
- Stassun K., Wood K., 1999, *ApJ* 510, 892
- Stassun K., Mathieu R.D., Mazeh T., Vrba F.J., 1999, *AJ*, in press
- Valenti J.A., Basri G., Johns C.M., 1993, *AJ* 106, 2024
- Vrba F.J., Chugainov P.F., Weaver W.B., Stauffer J.S., 1993, *AJ* 106, 1608
- Vrba F.J., Rydgren A.E., Chugainov P.F., Shakovskaia N.I., Weaver W.B., 1989, *AJ* 97, 483
- Walter F.M., Kuhl L.V., 1984, *ApJ* 284, 194
- Zickgraf F.J., Thiering I., Krautter J., 1997, *A&AS* 123, 103